Title

Point-of-care magnetic resonance technology to measure liver fat: Phantom and first-in-human pilot study

Journal

Magnetic Resonance in Medicine, 88(4)

ISSN

0740-3194

Authors

Barahman, Mark
Grunvald, Eduardo
Prado, Pablo J
et al.

Publication Date

2022-10-01

DOI

10.1002/mrm.29304

Peer reviewed

HHS Public Access

Author manuscript

Magn Reson Med. Author manuscript; available in PMC 2022 October 01.

Published in final edited form as:

Magn Reson Med. 2022 October ; 88(4): 1794–1805. doi:10.1002/mrm.29304.

POINT-OF-CARE MAGNETIC RESONANCE TECHNOLOGY TO MEASURE LIVER FAT: PHANTOM AND FIRST-IN-HUMAN PILOT STUDY

Mark Barahman[1,*], **Eduardo Grunvald**[2,3,*], **Pablo J. Prado**[4], **Alejandro Bussandri**[4], **Walter C. Henderson**[1], **Tanya Wolfson**[1], **Kathryn J. Fowler**[1], **Claude B. Sirlin**[1]

[1]Liver Imaging Group, Department of Radiology, University of California San Diego

[2]Division of General Internal Medicine, Department of Medicine, University of California San Diego

[3]Bariatric and Metabolic Institute, Division of Minimally Invasive Surgery, Department of Surgery, University of California San Diego

[4]Livivos Inc, San Diego CA

Abstract

Purpose: To assess feasibility and accuracy of Point-of-care (POC) NMR-PDFF in phantoms and in a human pilot study in a POC setting.

Methods: POC NMR (LiverScope, Livivos, San Diego CA) PDFF measurements were obtained of certified phantoms with known PDFF values (0–40%). In an IRB-approved, HIPAA-compliant prospective human study, a convenience sample of participants from an obesity clinic was enrolled (11/2020 to 06/2021). Inclusion criteria: body mass index (BMI) = 27– 40 kg/m^2, willingness to undergo POC NMR and MRI-PDFF measurements. Liver PDFF was measured by POC NMR and, within 35 days after, by a confounder-corrected chemical-shift-encoded MRI PDFF acquisition and reconstruction method. Adverse events were documented. Linear regression analyses were performed.

Results: POC NMR-PDFF measurements agreed with known phantom PDFF values (R^2=0.99). Fourteen participants were enrolled in the pilot human study. MRI-PDFF could not be obtained in 4 participants (claustrophobia reaction, n=3, exceeded size of MR scanner bore, n=1). POC NMR was unevaluable in 2 participants (insufficient signal penetration depth, n=1, failure to comply to instructions, n=1). Technical success was 11/13 (85%) for POC NMR PDFF.

In 7 participants (4 female; aged 31–74 years; median BMI 35 kg/m^2), MRI-PDFF (range 2.8–18.1%), and POC NMR-PDFF (range 3–25.2%), agreed with R^2=0.94. POC NMR had no adverse events.

Corresponding author: Claude B. Sirlin, M.D., Professor, Liver Imaging Group, Department of Radiology, University of California, San Diego, csirlin@health.ucsd.edu.

*Contributed equally to this work

Conclusion: POC NMR measures PDFF accurately in phantoms and, in a first-in-human pilot study, is feasible and accurate in adults with obesity. Further testing to determine precision and accuracy across larger and more diverse cohorts is needed.

Summary statement:

Point-of-care MR technology can quantify PDFF accurately in certified PDFF phantoms (R^2=0.99) and human adults with obesity and at risk for NAFLD (R^2=0.94).

Keywords

Hepatic steatosis; proton density fat fraction; point of care magnetic resonance; diffusion contrast

Introduction

Nonalcoholic fatty liver disease (NAFLD) is highly prevalent (1–3) and exerts tremendous economic strain on the world economy (4–6). This condition is progressive and may lead to steatohepatitis (NASH) and has been linked to cardiovascular disease, diabetes, cirrhosis, and cancer. Steatosis, a hallmark and initiating pathogenic feature, represents fat droplets in hepatocytes. The current noninvasive gold standard for steatosis assessment is chemical shift encoded (CSE) magnetic resonance imaging-based proton density fat fraction (MRI-PDFF). This biomarker quantifies liver fat and is used for clinical diagnosis and monitoring, and in pharmaceutical clinical trials. While accurate, MRI-PDFF is suboptimal for some applications due to high cost and limited availability as well as MRI contraindications such as claustrophobia. A well-tolerated point-of-care (POC) test that is accurate and reliable could enhance clinical diagnosis, facilitate clinical trial screening, and expand access to advanced diagnostic technology. Ultrasound (US) has point-of-care capability and can detect steatosis, but is not yet reliable for detecting lower levels of steatosis or for quantifying steatosis across its entire range (7–11).

POC NMR (LiverScope®, Livivos Inc., San Diego, CA) is a novel MR-based technology developed to measure PDFF, as well as other MR tissue properties, with POC capability (US20180220949 and US20190076080). The technology uses a custom-shaped open permanent magnet array (0.2 Tesla) integrated with a standard clinical gurney. Any room large enough to contain a gurney is adequate. Room shielding is not needed. To measure PDFF, a custom NMR pulse sequence is used while the patient lies on the gurney in the right-side down decubitus position. Signals from a ~8 cm diameter, 1 cm depth range in the liver 50 mm from the skin surface are collected. Fat and water signals are differentiated, and the PDFF calculated - as described in Methods.

Herein, the feasibility and accuracy of POC NMR-PDFF in phantoms and in a first-in-human pilot study was assessed. For the human study, adults with obesity were recruited, POC NMR in a point-of-care setting was performed, and PDFF was measured contemporaneously with magnitude-data confounder-corrected chemical-shift-encoded MRI (MRI-M) - as reference (12,13).

Methods

POC NMR fat fraction determination theory:

Traditional NMR-based fat fraction assessment relies on separation of fat and water signals based on their chemical shift. This can be accomplished with NMR spectroscopy, where fat and water signals are represented by different spectral peaks, or chemical-shift-encoded multi-gradient-echo imaging with appropriate echo spacing (14,15). These approaches must address confounding factors – such as spectral complexity, T1 bias, transverse relaxation bias, and other factors – for accurate PDFF determination.

POC NMR PDFF determination is based on a fundamentally different approach, diffusion contrast. As the diffusion coefficient of water is about 10 times higher than that of fat, a clear separation of water and fat signals may be attained by obtaining images over a range of b-values sufficient for this purpose. Clinical MRI systems cannot separate water and fat signals based on diffusivity differences because they cannot achieve this range of b-values. By comparison, POC NMR can generate fat-water diffusion contrast because it applies a strong constant field gradient able to produce sufficiently high b values (over 15,000 s/mm^2). To detect signals from fat and water, POC NMR applies a modified CPMG pulse sequence comprising a preparatory pulse followed by refocusing pulses with a 90-degree shifted phase. Phase cycling of the RF pulses and signal channels is performed to eliminate spurious signals. T2 is measured in the time series during CPMG acquisition and incorporated into the signal model. Although perfusion is a known confounder of ADC of water, this is not relevant to the PDFF estimation approach used here because only fat / water contrast is required for the calculation. The water perfusion and water diffusion components need not be separated. To minimize the effects of bulk motion on signal amplitude, acquisitions were taken during breath holds (to minimize respiratory motion) and with the patient positioned right side down (to minimize effects of cardiac motion on the right lobe of the liver). Unlike spectroscopy and chemical-shift-encoded MR imaging, there is no need for spectral modeling because the fat and water NMR signals are separated based on a physical property that applies to entire fat or water molecules (diffusivity), not on a chemical property that applies to individual hydrogen protons within those molecules (chemical shift).

Diffusion Contrast—As the diffusion coefficient of liver water is approximately 1×10^{-3} mm^2/s, which is on the order of 10 times higher than that of fat, a clear separation (partial or complete) of the NMR responses may be attained. The differentiation of the signals is achieved by NMR measurements in the presence of a static high field gradient (G) with CPMG pulse sequences with different inter pulse spacing or with a CPMG sequence with a diffusion encoding preparation stage. Phase cycling of the RF pulses and signal channels is performed to eliminate unwanted spurious signals (Figure 1).

In the phantom and in-vivo studies described in the present manuscript, the signal amplitude at varying diffusion encoding times is used to compute the relative amount of fat and water. The signal decay in a CPMG sequence in the presence of a field gradient depends on the inter echo spacing. The higher the diffusion coefficient, the faster the decay (16). An effective way to achieve diffusion encoding is by applying a number of “preparation pulses” followed by a Hann or multi-echo (e.g. CPMG) sequence. The diffusion encoding times can

be varied to adjust the b value, while the time parameters of the CPMG sequence are not changed.

Diffusion Contrast Confounders—The POC NMR sequence is designed to address potential confounders. T1 bias is minimized by utilizing a recycling delay (~1000ms) about 5x longer than the T1 of liver water at 0.2T (~200ms) (17–19). It minimizes potential confounding effects of perfusion by performing rapid acquisitions (μs timescale) that are sensitive only to diffusion, not perfusion. It minimizes T2* decay effects by applying refocusing pulses and calculating T2 at spin echo peaks (Figure 1) to calculate the T2. Unlike spectroscopy and chemical-shift-encoded MR imaging, there is no need for spectral modeling because the fat and water NMR signals are separated based on a physical property that applies to entire fat or water molecules (diffusivity), not on a chemical property that applies to individual hydrogen protons within those molecules (chemical shift). Transverse relaxation is not a confounder because the signal amplitude is determined at the zero-crossing point in the time series, so the measurement is effectively independent of T2.

POC NMR PDFF calculation—The NMR signal amplitude decreases as a function of the diffusion encoding time (TD). A b value is used to scale the time series with the static field gradient, G (16).

$$b = \frac{\gamma^2 G^2 TD^3}{12}$$

where γ, the gyromagnetic ratio of proton spins = 267,520,000 rad/(sT)

G = 1.875 T/m for the current version of the device, at the chosen operating depth, and therefore, for the diffusion encoding times used in the pulse sequence:

$$b\ range = 20 - 15,000\ s/mm^2$$

For reference, clinical MRI scanners utilize transient gradient magnetic fields with amplitudes of 30 – 45 mT/m giving b values ~500 – 1000 s/mm^2. This allows POC NMR to observe molecular dynamic effects over a wider time-scale range than clinical MRI instruments. For example – as shown below, signals from water and fat can be clearly separated based on their diffusion coefficients.

For the pulse sequence shown in Figure 1, the signal amplitude for the first echo is a function of the initial pulse separation. Then, each echo in the CPMG section decays exponentially. In the case of a signal generated by fat and water proton signals, the decay is represented by a double exponential decay.

To increase signal to noise ratio (SNR), the diffusion encoding sequence is repeated and the signal is averaged. For random Gaussian noise, when the repetition is performed after the spins are fully polarized (long recycling delay), the SNR increases approximately as the square root of the number of repetitions.

For a recycling delay, or time between sequences *rd*, the NMR signal amplitude (A) at a time t along the CPMG time series for a diffusion encoding time (TD), is

$$\begin{aligned} \mathrm{A(b,t)} = \mathrm{A_W(b=0,t=0)e}^{-D_w b}\mathrm{e}^{-\frac{t}{T2_w}}\left(1-\mathrm{e}^{-\frac{rd}{T1_w}}\right) \\ + \mathrm{A}_f\mathrm{(b=0,t=0)e}^{-D_f b}\mathrm{e}^{-\frac{t}{T2_f}}\left(1-\mathrm{e}^{-\frac{rd}{T1_f}}\right) \end{aligned}$$

$A_w(b=0, t=0)$ is the signal amplitude of the first echo (t=0) from water protons when there is no diffusion encoding (b = 0). This is proportional to the concentration of protons in water. In a similar way for fat protons, $A_f(b=0, t=0)$. The Proton Density Fat Fraction is,

$$PDFF = 100\%\frac{A_{fat}(b=0,\ t=0)}{A_{fat}(b=0,\ t=0)+A_{water}(b=0,\ t=0)}$$

For full polarization prior to repeating the pulse sequence, or rd $\gg$ $T1_f$ and $T1_w$,

$$\mathrm{A(b,t)} = A_{\mathrm{water}}\,\mathrm{(b=0,t=0)e}^{-D_w b}\mathrm{e}^{-\frac{t}{T2_w}} + A_{\mathrm{fat}}\mathrm{(b=0,t=0)e}^{-D_f b}\mathrm{e}^{-\frac{t}{T2_f}}$$

In this case, no T1 correction is necessary.

It is observed that for fast CPMG sequences without diffusion encoding the total (water and fat) signal at time t is,

$$\mathrm{A(b=0,t)} = A_{water}\mathrm{(b=0,t=0)e}^{-t/T2_w} + A_{fat}\mathrm{(b=0,t=0)e}^{-t/T2_f}$$

For long diffusion encoding times where $\frac{1}{\mathrm{Df}} > \sim \mathrm{b} > > \frac{1}{D_w}$, only the fat signal is observed,

$$\mathrm{A(b,t)} = \mathrm{A_{fat}(b,t)} = \mathrm{A_{fat}\,(b=0,t=0)e}^{-\mathrm{Df}\mathrm{b}}\mathrm{e}^{-t/T2_f}$$

By collecting the diffusion-encoded NMR signals at various encoding times (b values), the PDFF and diffusion coefficients for water and fat are computed. At each b value the CPMG time series is represented by a double exponential decay, with $T2_f$ and $T2_w$ relaxation times.

POC NMR device design:

The POC NMR device is a custom-shape compact, open-magnet and radiofrequency antenna that generates a sensitive volume in a remote area outside of the sensing probe. In this study, we used a prototype magnet that was 35 cm wide with a maximum field strength of 210 mT at 35mm depth. To perform measurement at a gradient of 1.875 T/m, an operating depth of 50mm was chosen. Coupled with this magnet, the modified CPMG sequence acquired signals from a discoid volume 8 cm in diameter, 1 cm thick. The volume interrogated by POC NMR is approximately 10 cm^3 (estimated by Bloch equation (20)) and can be modified

by changing the duration of the excitation pulse. The experimental parameters used are given in Table 1.

Study design:

This pilot project included a phantom study and an IRB-approved, HIPAA-compliant, prospective, first-in-human study. POC NMR PDFF measurements were compared to known PDFF values (phantom study) or to contemporaneous MRI-M PDFF measurements (human study).

Phantom study: Four certified PDFF phantoms (Calimetrix, LLC, Madison, WI), with known PDFF values from 10 to 40%, and a pure water phantom, representing 0% PDFF, were positioned above the POC NMR probe, centered with the flat antenna element, ensuring the sensitive volume was inside of the phantom (Figure 2). POC NMR-PDFF measurements for the phantom study were made using a modified CPMG pulse sequence as explained above.

Human pilot study: For the human study (IRB # 201164), a convenience sample size of 14 adults was chosen based on feasibility and precedence of prior published pilot studies of this type (21). Adult participants were recruited from the University of California, San Diego Bariatric and Metabolic Institute, between November 2020 and June 2021. Obese participants are at risk for having liver steatosis, but also have an expected wide range of liver fat, including normal (22). Further, obese participants constitute a technically challenging study population and validation in obese participants can be extended to validation in non-obese individuals. Inclusion criteria were: age ≥ 18 years; known or suspected NAFLD based on prior liver biopsy or clinical data (such as diabetes, hyperlipedemia, or other components of metabolic syndrome in absence of excess alcohol intake and other liver diseases), and body mass index (BMI) = 27–40 kg/m^2. Potential participants were excluded if they were pregnant or trying to become pregnant, or if they had a contraindication to MRI. After providing informed consent, enrolled participants underwent anthropometric measurements (weight and height were measured by a medical assistant, and waist circumference was measured by a physician), a POC NMR examination in a clinic room within the bariatric center (see below) and, within 35 days after, an MRI examination on a full-body clinical system (see below).

POC NMR-PDFF Exams: The prototype POC NMR device was placed in a standard clinic room in the UCSD bariatric and metabolic institute. Participants were positioned in the right decubitus position (Figure 3). The center of the POC NMR probe was aligned with the participant's xiphoid process and POC NMR measurements were obtained and interpreted for PDFF by trained personnel. The NMR response was attained for phase-cycled CPMG-like sequences using 24 separate b values (20–15,000 s/mm^2 used in human experiments) and a short excitation pulse. Each b value was obtained during a separate 6-second breath hold. Inter-acquisition spacing was several seconds. Total examination time for the preliminary protocol used in this study, including initial set up, positioning, b-value acquisitions, and pauses between acquisitions was ~ 20 min. Total active acquisition time was <3 min.

POC NMR-PDFF analysis: The amplitude of the NMR signal was measured for a series of diffusion encoding times (b values) (Figure 4A). To increase sensitivity, a train of refocusing pulses was added after the diffusion encoding stage of the pulse sequence (Figure 1). The contributions of water and fat protons to the measured signal were separated based on diffusion coefficients. These contributions were used to compute the PDFF.

MRI-PDFF Exams:

Image Acquisition: MRI exams were performed on enrolled participants by trained MR technologists at our institution's Clinical and Translational Research Institute using a clinical 3T MRI scanner (GE Signa Discovery MR750, GE Healthcare, Waukesha, WI) with a 32-channel phased-array torso coil centered over the liver. Participants were positioned in the scanner feet first and supine. Following a 3-plane localizer, a confounder-corrected chemical-shift encoding 2D MRI sequence was performed. The sequence uses a low flip angle (10°) relative to TR (150 ms) to minimize T1 effects and acquires six spoiled gradient echoes at evenly-spaced, nominally out-of-phase and in-phase echo times (TEs) from 1.15 to 6.9 ms were used to permit chemical-shift-based separation of fat and water signals and correction for R2* signal decay. Slices were prescribed to cover the entire liver in a single breath-hold of 20 seconds.

MRI-PDFF postprocessing: Parametric MRI-PDFF maps were generated by the scanner computer which applied a custom algorithm pixel-by-pixel to the source images (23). The algorithm assumes exponential R2* signal decay across the TEs and models water as a single peak at 4.7 ppm with fat being a multi-component signal with relative amplitudes 0.047, 0.039, 0.006, 0.120, 0.700, and 0.088 at 5.30, 4.20, 2.75, 2.10, 1.30, 0.90 ppm, respectively (24).

MRI-PDFF analysis: A trained image analyst placed a 1-cm radius ROI in each of the nine liver segments as previously described (25) (Figure 4B). The 9-segment average liver PDFF was computed and reported.

Skin-capsule distance (SCD) calculation: An image analyst manually measured the SCD using the MR images with the following approach: The 3-plane localizer was used to identify the table positions of the superior and inferior liver edges. The center location was calculated using the table position arithmetic mean. On the axial PDFF slice that corresponded most closely to that center location, the analyst identified the coordinates of the anterior and posterior edges of the liver. The middle location was found using the arithmetic mean. The SCD was then measured as the shortest horizontal line from the middle location of the liver capsule edge to the skin edge.

Statistical analysis: For both the phantom and human study, a Bland-Altman analysis was performed and the following Quantitative Imaging Biomarkers Alliance (QIBA)-advocated agreement metrics were calculated: bias and its significance, limits of agreement (LOA), reproducibility coefficient (RDC), intra-class correlation (ICC) and paired data coefficient of variation (CV) (26). Linear regression was used to model reference MRI-PDFF values (known values in phantom studies, chemical-shift-encoded MRI-derived values in human

studies) as a function of investigational POC NMR-PDFF values. Goodness-of-fit (R^2), slope, and intercept of the regression model were reported. Additionally for the human study, the patient sample was summarized descriptively.

Results

POC NMR accuracy with PDFF phantoms

Goodness of fit for the manufacturer certified PDFF vs LiverScope PDFF model was R^2 = 0.99 (Figure 5-left panel), demonstrating a high level of agreement. The regression equation is Phantom PDFF=1.03*POC NMR PDFF + 0.76. A Bland-Altman analysis (Figure 5-right panel) shows the ICC is 0.99, the RDC is 3.09% and the LOA are (−1.81, 4.37).

Human POC NMR study

Study participants—Fourteen participants with obesity were enrolled (Figure 6). One participant withdrew prior to any imaging procedures. The remaining 13 participants underwent at least one attempted imaging procedure (Table 2). One participant underwent POC NMR only and was lost to follow up prior to scheduling MRI. Twelve participants underwent both MRI and POC NMR. In one of these 12 participants (ID #11), POC NMR failed due to body habitus preventing acquisition of signals from the liver. The signal response in this participant was visually consistent with adipose tissue, indicating that the interrogated volume comprised only subcutaneous or visceral fat. The SCD was not measured in this participant because they were lost to follow up and did not undergo an MRI exam. One participant could not comply with the instructions, resulting in unevaluable POC NMR data (ID #3). Notably, this participant underwent MRI and the results were evaluable. Four participants did not complete MRI exams: three due to claustrophobia reactions that prohibited exam completion (ID #4,6,8) and one who could not enter the scanner due to girth exceeding bore diameter (ID #13). Thus, technical success was 11/13 (85%) for POC NMR PDFF and 8/12 (67%) for MRI PDFF.

The seven participants with evaluable contemporaneous MRI-PDFF and POC NMR PDFF measurements were included in the accuracy analysis (Table 2). Four (57%) were female. Their ages ranged from 31 to 74 years, and their median BMI was 35.4 kg/m^2. Median time interval from MRI to POC NMR exam was 18 days (range 7–35 days).

POC NMR accuracy with reference to MRI-PDFF—MRI-PDFF measurements ranged from 2.8% to 18.1% (median 11.05%). POC NMR-PDFF measurements ranged from 3% to 25.2% (median 10.2%). The MRI PDFF vs. LiverScope PDFF linear regression model (Figure 7-left panel) shows adjusted R^2 = 0.94. The regression equation is MRI_PDFF = 1.15*POC NMR_PDFF - 1.46. Bland-Altman analysis of MRI-PDFF and POC NMR-PDFF (Figure 7-right panel) shows no bias with limits of agreement of −2.45%, 2.57%. The ICC with 95% confidence interval is 0.97 [0.83, 0.99], CV=9.35%, RDC = 2.51%. Figure 4 illustrates PDFF measurements made by POC NMR and chemical-shift-encoded MRI in a 31-year old adult with BMI of 35.9 kg/m^2.

Discussion

Point-of-care NMR was investigated as an approach for liver fat quantification in a pilot and feasibility study. In certified PDFF phantoms, POC NMR PDFF agreed closely with ground-truth PDFF values (R^2 = 0.99). In human adults with obesity and at risk for NAFLD, POC NMR performed in a point-of-care setting was feasible and agreed closely with contemporaneous MRI-PDFF reference standard values (R^2 = 0.94) (10,23,25,27–32) POC NMR was well tolerated and no associated adverse events were reported. By comparison, three participants had claustrophobia reactions during MRI resulting in exam termination before PDFF sequences acquisition. This rate of claustrophobia reactions in this study (23%) is high compared to other studies even considering previous reports measuring the rate of claustrophobia reactions in MRI exams to be as high as 15% (33–35). This observation is likely an effect of the small sample size and should not be used to make final conclusions regarding the technical success of MRI PDFF.

This was a first-in-human feasibility trial of this POC NMR device. POC NMR was technically successful in 11 of 13 participants. To place this into context, MRI was successful in 8 of 12 participants, although the study was too small and not designed to compare the technical success rate of these two methodologies. Of the two participants who failed POC NMR exams, one was not able to comply with the exam, preventing adequate data collection. This participant had evaluable MRI PDFF. One participant had technical failure due to insufficient penetration of the device. This is evident as the measured NMR parameters are characteristic of adipose tissue and not liver fat and water. SCD was not calculated for this participant because were lost to follow up when attempting to schedule the MRI exam. Without associated imaging, the exact measurement location cannot be determined by POC NMR, so the NMR signal is evaluated to determine if the measurement is collected in the liver. Additionally, measurement could be affected by lesions or other large structures in the measured area. Such lesions were not observed in this study but in future studies we will examine the corresponding portion of the liver on contemporaneous MRI to assess the frequency of lesions such as large cysts in the area.

These results suggest that the current prototype is adequate for measuring liver fat in obese adults with a supine SCD up to about 5.8 cm. The supine SCD is likely significantly longer than the SCD using right side down decubitus positioning which is used for POC NMR measurements. To investigate maximum penetration depth in humans, future studies will evaluate the SCD in the same position used for POC NMR measurements. Participants with obesity can be especially challenging for POC methods due to limited signal penetration of such devices. The positive correlation reported here demonstrates the feasibility of this technology in this technically challenging patient population. Increased penetration depth may be necessary to enable POC NMR measurements in severely obese patients. This may require future modifications of the antenna geometry and transmitter design, as well as further optimization of the pulse sequence.

Several POC methodologies for measurement of liver fat are in clinical use or development. US is an attractive modality for POC determination of liver fat. It is relatively low cost and does not involve ionizing radiation. However, qualitative US relies on subjective measures

of steatosis including near field echogenicity, and (due to fat attenuation) blurring of deep structures. Imaging is limited in patients with obesity, reported accuracy is relatively low (especially for low steatosis grades) and there is high reader variability (7–9). Quantitative US (QUS) may potentially address subjectivity and variability by analyzing radiofrequency data to derive objective measures such as the attenuation and backscatter coefficients (9). Correlation between QUS-derived parameters and MRI PDFF has been reported to be ρ=0.69 (9), r=0.85 (10), and ρ=0.82 (11) in recent studies. Our preliminary study suggests that the correlation between POC NMR and MRI-PDFF may be higher, though further validation is required. Compared to QUS, POC NMR has the added advantage of producing an absolute fat fraction quantification rather than indirect parameters such as controlled attenuation parameter.

The leading magnetic resonance-based approach for PDFF quantification is CSE-MRI. This technology is available on clinical scanners and offers a wide dynamic range with a high degree of accuracy for detection of steatosis (AUROC 0.99), and has been validated in animal and human studies for quantifying fat content using biopsy and MRS as the reference standard (36). MRI PDFF can be obtained using MRI magnitude (MRI-M) or MRI complex (MRI-C) measurements. The ICC between MRI-M and MRI-C for the 9-segment average is 0.995 (37) and between MRI and MRS is 0.987–0.998 depending on the flip angle used (38). In fat-water phantoms evaluated with MRI-PDFF across 6 sites, 3 device manufacturers, and 2 field strengths, the ICC was 0.999 (39). The ICC reported here for the human study using POC NMR is 0.97. Moreover, in a meta-analysis comparing MRI to MRS, including 3191 PDFF measurements in 1679 subjects, the LOA were (−3.95, +3.70). Similarly, the LOA in the present study were (−2.45, +2.57), indicating comparable precision. An important difference between MRI and POC NMR is that MRI evaluates the entire liver, while POC NMR only evaluates a volume (~10 cm^3) in the right lobe. Therefore, heterogenous liver fat deposition may confound conclusions of the measurement. However, this is also the case for biopsy (~10–20 mm^3) (40) and commercial POC ultrasound devices evaluating controlled attenuation parameter (~ 3 cm^3) (41). Compared to MRI-PDFF measured on clinical scanners, POC NMR may offer unique advantages such as the small size and open design, which avoids issues with claustrophobic patients, a problem that affected 3 of our participants in this study. In addition, it is potentially widely available due to lower cost, and ease of use.

This pilot study is limited in the size and PDFF range in the human study cohort. Only 7 participants had evaluable POC NMR PDFF and MRI PDFF measurements. The small sample size leads to some statistical uncertainty. There is no in-vivo PDFF data above 18% and this dataset only has two points in the low range of liver fat. Repeatability is also important but was not assessed in the current study. Finally, the potential confounding effects of primary liver pathology were not studied. Study participants were recruited from an obesity clinic to assure a wide PDFF distribution without substantial primary liver disease. POC NMR should be validated in a study population with a range of primary hepatic diseases. Future studies are being planned to sufficiently power accuracy and precision analysis with a larger cohort, a wider PDFF range, and a wider spectrum of primary hepatic diseases. This will enable evaluation of accuracy and linearity for low, intermediate, and high PDFF measurements and the assessment of possible confounders

in the target population. Test-retest repeatability will be measured by obtaining multiple scans per participant with participant repositioning. The total test time using the preliminary algorithm used in this study was 20 minutes, which is comparable to MRI. Studies are ongoing to optimize the acquisition such that all necessary data is acquired within a single breath hold. This study evaluated POC NMR PDFF as the only biomarker. But POC NMR potentially can measure other MRI properties, such as diffusion coefficients and relaxation values, which have been shown to have diagnostic value (42–44). Future work will assess the accuracy and biological or clinical relevance of these other measurements, especially as they pertain to liver fibrosis and inflammation. The pulse sequence used in POC NMR can be further modified to optimize for shorter examination times, for example the number of b values scanned could be reduced to 3 or 4 and the echo train length may be reduced, optimizing for test duration with a threshold sensitivity or precision.

Conclusions

POC NMR is a point of care device that shows high agreement with MRI-PDFF in both phantoms and human participants. Preliminary results are encouraging. Further research to establish reproducibility and accuracy over a wider range of PDFF values is needed to validate this new technology.

Works Cited

1. Williams CD, Stengel J, Asike MI, et al. Prevalence of nonalcoholic fatty liver disease and nonalcoholic steatohepatitis among a largely middle-aged population utilizing ultrasound and liver biopsy: A prospective study. Gastroenterology 2011;140:124–131 doi: 10.1053/j.gastro.2010.09.038. [PubMed: 20858492]
2. Vernon G, Baranova A, Younossi ZM. Systematic review: The epidemiology and natural history of non-alcoholic fatty liver disease and non-alcoholic steatohepatitis in adults. Aliment. Pharmacol. Ther 2011;34:274–285 doi: 10.1111/j.1365-2036.2011.04724.x. [PubMed: 21623852]
3. Lazo M, Hernaez R, Eberhardt MS, et al. Prevalence of nonalcoholic fatty liver disease in the United States: The third national health and nutrition examination survey, 1988–1994. Am. J. Epidemiol 2013;178:38–45 doi: 10.1093/aje/kws448. [PubMed: 23703888]
4. Younossi ZM, Blissett D, Blissett R, et al. The economic and clinical burden of nonalcoholic fatty liver disease in the United States and Europe. Hepatology 2016;64:1577–1586 doi: 10.1002/hep.28785. [PubMed: 27543837]
5. Romero-Gomez M, Kachru N, Zamorano MA, Darba J, Shreay S. Disease severity predicts higher healthcare costs among hospitalized nonalcoholic fatty liver disease/nonalcoholic steatohepatitis (NAFLD/NASH) patients in Spain. Medicine (Baltimore). 2020;99:e23506 doi: 10.1097/MD.0000000000023506. [PubMed: 33327291]
6. Younossi ZM, Tampi RP, Racila A, et al. Economic and clinical burden of nonalcoholic steatohepatitis in patients with type 2 diabetes in the U.S. Diabetes Care 2020;43:283–289 doi: 10.2337/dc19-1113. [PubMed: 31658974]
7. Özcan HN, Oğuz B, Haliloğlu M, Orhan D, Karçaaltıncaba M. Imaging patterns of fatty liver in pediatric patients. Diagnostic Interv. Radiol 2015;21:355–360 doi: 10.5152/dir.2015.14505.
8. Ozturk A, Grajo JR, Gee MS, et al. Quantitative Hepatic Fat Quantification in Non-alcoholic Fatty Liver Disease Using Ultrasound-Based Techniques: A Review of Literature and Their Diagnostic Performance. Ultrasound Med. Biol 2018;44:2461–2475 doi: 10.1016/j.ultrasmedbio.2018.07.019. [PubMed: 30232020]
9. Paige JS, Bernstein GS, Heba E, et al. A pilot comparative study of quantitative ultrasound, conventional ultrasound, and MRI for predicting histology-determined steatosis grade in

adult nonalcoholic fatty liver disease. Am. J. Roentgenol 2017;208:W168–W177 doi: 10.2214/AJR.16.16726. [PubMed: 28267360]

10. Han A, Byra M, Heba E, et al. Noninvasive diagnosis of nonalcoholic fatty liver disease and quantification of liver fat with radiofrequency ultrasound data using one-dimensional convolutional neural networks. Radiology 2020;295:342–350 doi: 10.1148/radiol.2020191160. [PubMed: 32096706]
11. Han A, Zhang YN, Boehringer AS, et al. Assessment of hepatic steatosis in nonalcoholic fatty liver disease by using quantitative US. Radiology 2020;295:106–113 doi: 10.1148/radiol.2020191152. [PubMed: 32013792]
12. Yokoo T, Bydder M, Hamilton G, et al. Diagnostic and Fat-Grading Accuracy of low-flip-angle multiecho gradient recalled echo MR Imaging at 1.5T. Radiology 2009;251:67–76. [PubMed: 19221054]
13. Yokoo T, Shiehmorteza M, Hamilton G, et al. Estimation of hepatic proton-density fat fraction by using MR imaging at 3.0 T. Radiology 2011;258:749–759 doi: 10.1148/radiol.10100659. [PubMed: 21212366]
14. BUXTON RB, WISMER GL, ROSEN BR, et al. Quantitative proton chemical-shift imaging. Magn. Reson. Med. Off. J. Soc. Magn. Reson. Med 3:881–900.
15. Hussain HK, Chenevert TL, Londy FJ, et al. Hepatic fat fraction: MR imaging for quantitative measurement and display - Early experience. Radiology 2005;237:1048–1055 doi: 10.1148/radiol.2373041639. [PubMed: 16237138]
16. Ninla Elmawati Falabiba. Single-Sided NMR. (Casanova F, Perlo J, Blümich B, editors.) Berlin, Heidelberg: Springer Berlin Heidelberg; 2011. doi: 10.1007/978-3-642-16307-4.
17. Thomsen C, Becker U, Winkler K, Christoffersen P, Jensen M, Henriksen O. Quantification of liver fat using magnetic resonance spectroscopy. Magn. Reson. Imaging 1994;12:487–495 doi: 10.1016/0730-725X(94)92543-7. [PubMed: 8007779]
18. Doyle F, Pennock J, Banks L, et al. Nuclear magnetic resonance imaging of the liver: initial experience. Am. J. Roentgenol 1982;138:193–200 doi: 10.2214/ajr.138.2.193. [PubMed: 6275694]
19. Leporq B, Ratiney H, Pilleul F, Beuf O. Liver fat volume fraction quantification with fat and water T1 and T2*estimation and accounting for NMR multiple components in patients with chronic liver disease at 1.5 and 3.0 T. Eur. Radiol 2013;23:2175–2186 doi: 10.1007/s00330-013-2826-x. [PubMed: 23588583]
20. Bloch F Nuclear induction. Phys. Rev 1946;70:460–474 doi: 10.1103/PhysRev.70.460.
21. Thomaides-Brears HB, Lepe R, Banerjee R, Duncker C. Multiparametric MR mapping in clinical decision-making for diffuse liver disease. Abdom. Radiol 2020;45:3507–3522 doi: 10.1007/s00261-020-02684-3.
22. Luyckx FH, Desaive C, Thiry A, et al. Liver abnormalities in severely obese subjects: Effect of drastic weight loss after gastroplasty. Int. J. Obes 1998;22:222–226 doi: 10.1038/sj.ijo.0800571.
23. Tang A, Tan J, Sun M, et al. Nonalcoholic fatty liver disease: MR imaging of liver proton density fat fraction to assess hepatic steatosis. Radiology 2013;267:422–431 doi: 10.1148/radiol.12120896. [PubMed: 23382291]
24. Hamilton G, Yokoo T, Bydder M, et al. In vivo characterization of the liver fat 1H MR spectrum. NMR Biomed. 2011;24:784–790 doi: 10.1002/nbm.1622. [PubMed: 21834002]
25. Mamidipalli A, Fowler KJ, Hamilton G, et al. Prospective comparison of longitudinal change in hepatic proton density fat fraction (PDFF) estimated by magnitude-based MRI (MRI-M) and complex-based MRI (MRI-C). Eur. Radiol 2020;30:5120–5129 doi: 10.1007/s00330-020-06858-x. [PubMed: 32318847]
26. Raunig DL, McShane LM, Pennello G, et al. Quantitative imaging biomarkers: A review of statistical methods for technical performance assessment. Stat. Methods Med. Res 2015;24:27–67 doi: 10.1177/0962280214537344. [PubMed: 24919831]
27. Yokoo T, Serai SD, Pirasteh A, et al. Linearity, bias, and precision of hepatic proton density fat fraction measurements by using MR imaging: A meta-analysis. Radiology 2018;286:486–498 doi: 10.1148/radiol.2017170550. [PubMed: 28892458]

28. Ajmera VH, Liu A, Singh S, et al. Clinical Utility of an Increase in Magnetic Resonance Elastography in Predicting Fibrosis Progression in Nonalcoholic Fatty Liver Disease. Hepatology 2020;71:849–860 doi: 10.1002/hep.30974. [PubMed: 31556124]
29. Caussy C, Reeder SB, Sirlin CB, Loomba R. Noninvasive, Quantitative Assessment of Liver Fat by MRI-PDFF as an Endpoint in NASH Trials. Hepatology 2018;68:763–772 doi: 10.1002/hep.29797. [PubMed: 29356032]
30. Hamilton G, Schlein AN, Wolfson T, et al. The relationship between liver triglyceride composition and proton density fat fraction as assessed by 1H MRS. NMR Biomed. 2020;33:1–8 doi: 10.1002/nbm.4286.
31. Hooker JC, Hamilton G, Park CC, et al. Inter-reader agreement of magnetic resonance imaging proton density fat fraction and its longitudinal change in a clinical trial of adults with nonalcoholic steatohepatitis. Abdom. Radiol 2019;44:482–492 doi: 10.1007/s00261-018-1745-3.
32. Bonekamp S, Tang A, Mashhood A, et al. Spatial distribution of MRI-determined hepatic proton density fat fraction in adults with nonalcoholic fatty liver disease. J. Magn. Reson. Imaging 2014;39:1525–1532 doi: 10.1002/jmri.24321. [PubMed: 24987758]
33. Nguyen XV, Tahir S, Bresnahan BW, et al. Prevalence and Financial Impact of Claustrophobia, Anxiety, Patient Motion, and Other Patient Events in Magnetic Resonance Imaging. Top. Magn. Reson. Imaging 2020;29:125–130 doi: 10.1097/RMR.0000000000000243. [PubMed: 32568974]
34. Napp AE, Enders J, Roehle R, et al. Analysis and Prediction of Claustrophobia during MR Imaging with the Claustrophobia Questionnaire: An Observational Prospective 18-month Single-Center Study of 6500 Patients. Radiology 2017;283:148–157 doi: 10.1148/radiol.2016160476. [PubMed: 27892781]
35. Kieran KJ, Brunbergz JA. Adult claustrophobia, anxiety and sedation in MRI. Magn. Reson. Imaging 1997;15:51–54 doi: 10.1016/S0730-725X(96)00351-7. [PubMed: 9084025]
36. Starekova J, Reeder SB. Liver fat quantification: where do we stand? Abdom. Radiol 2020;45:3386–3399 doi: 10.1007/s00261-020-02783-1.
37. Haufe WM, Wolfson T, Hooker CA, et al. Accuracy of PDFF estimation by magnitude-based and complex-based MRI in children with MR spectroscopy as a reference. J. Magn. Reson. Imaging 2017;46:1641–1647 doi: 10.1002/jmri.25699. [PubMed: 28323377]
38. Johnson BL, Schroeder ME, Wolfson T, et al. Effect of flip angle on the accuracy and repeatability of hepatic proton density fat fraction estimation by complex data-based, T1-independent, T2-corrected, spectrum-modeled MRI. J. Magn. Reson. Imaging 2014;39:440–447 doi: 10.1002/jmri.24153. [PubMed: 23596052]
39. Hernando D, Sharma SD, Aliyari Ghasabeh M, et al. Multisite, multivendor validation of the accuracy and reproducibility of proton-density fat-fraction quantification at 1.5T and 3T using a fat–water phantom. Magn. Reson. Med 2017;77:1516–1524 doi: 10.1002/mrm.26228. [PubMed: 27080068]
40. Inal GH, Öztekin VÇ, Uğurlu Ö, Kosan M, Akdemir Ö, Çetinkaya M. Sixteen gauge needles improve specimen quality but not cancer detection rate in transrectal ultrasound-guided 10-core prostate biopsies. Prostate Cancer Prostatic Dis 2008;11:270–273 doi: 10.1038/pcan.2008.34. [PubMed: 18521101]
41. Pirmoazen AM, Khurana A, Kaffas A El, Kamaya A. Quantitative ultrasound approaches for diagnosis and monitoring hepatic steatosis in nonalcoholic fatty liver disease. Theranostics 2020;10:4277–4289 doi: 10.7150/thno.40249. [PubMed: 32226553]
42. Bachtiar V, Kelly MD, Wilman HR, et al. Repeatability and reproducibility of multiparametric magnetic resonance imaging of the liver. PLoS One 2019;14:1–12 doi: 10.1371/journal.pone.0214921.
43. Dennis A, Kelly MD, Fernandes C, et al. Correlations Between MRI Biomarkers PDFF and cT1 With Histopathological Features of Non-Alcoholic Steatohepatitis. Front. Endocrinol. (Lausanne) 2021;11:1–10 doi: 10.3389/fendo.2020.575843.
44. Selvaraj EA, Mózes FE, Jayaswal ANA, et al. Diagnostic accuracy of elastography and magnetic resonance imaging in patients with NAFLD: A systematic review and meta-analysis. J. Hepatol 2021;75:770–785 doi: 10.1016/j.jhep.2021.04.044. [PubMed: 33991635]

Key results:

Point-of-care (POC) NMR is a novel technology for liver fat quantification.

- POC NMR PDFF agreed closely with ground-truth PDFF values in commercial PDFF phantoms ($R^2 = 0.99$)
- POC NMR was feasible in an outpatient clinic, had no demonstrated adverse events, and agreed closely with contemporaneous MRI-PDFF reference standard values ($R^2 = 0.94$) in human adults with obesity and at risk for NAFLD

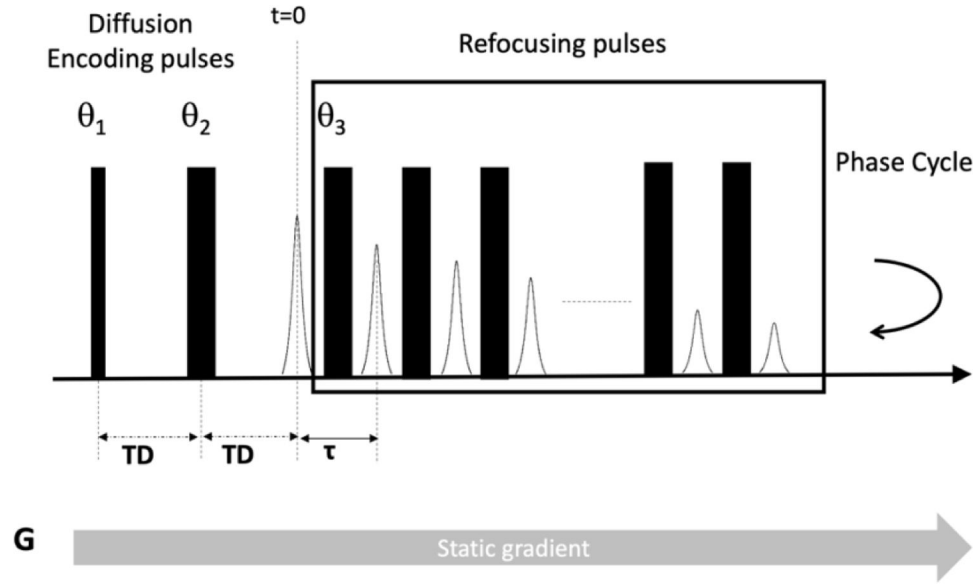

Figure 1.

Diffusion encoding pulse sequence used in POC NMR. Excitation pulse (Θ_1) and refocusing pulses (Θ_2) generate a diffusion-weighed echo, followed by a train of refocusing pulses, Θ_3. TD= diffusion encoding time, which is changed to achieve different b values. τ= inter echo spacing time during refocusing pulse sequence. Figure adapted from (16) with modification.

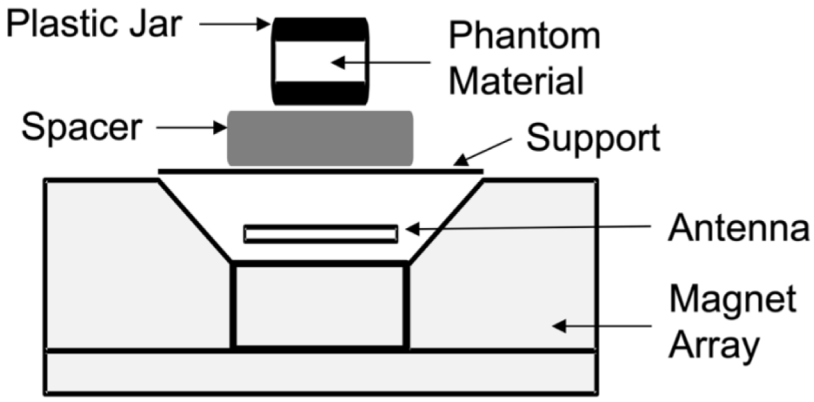

Figure 2.
POC NMR measurement of PDFF phantoms

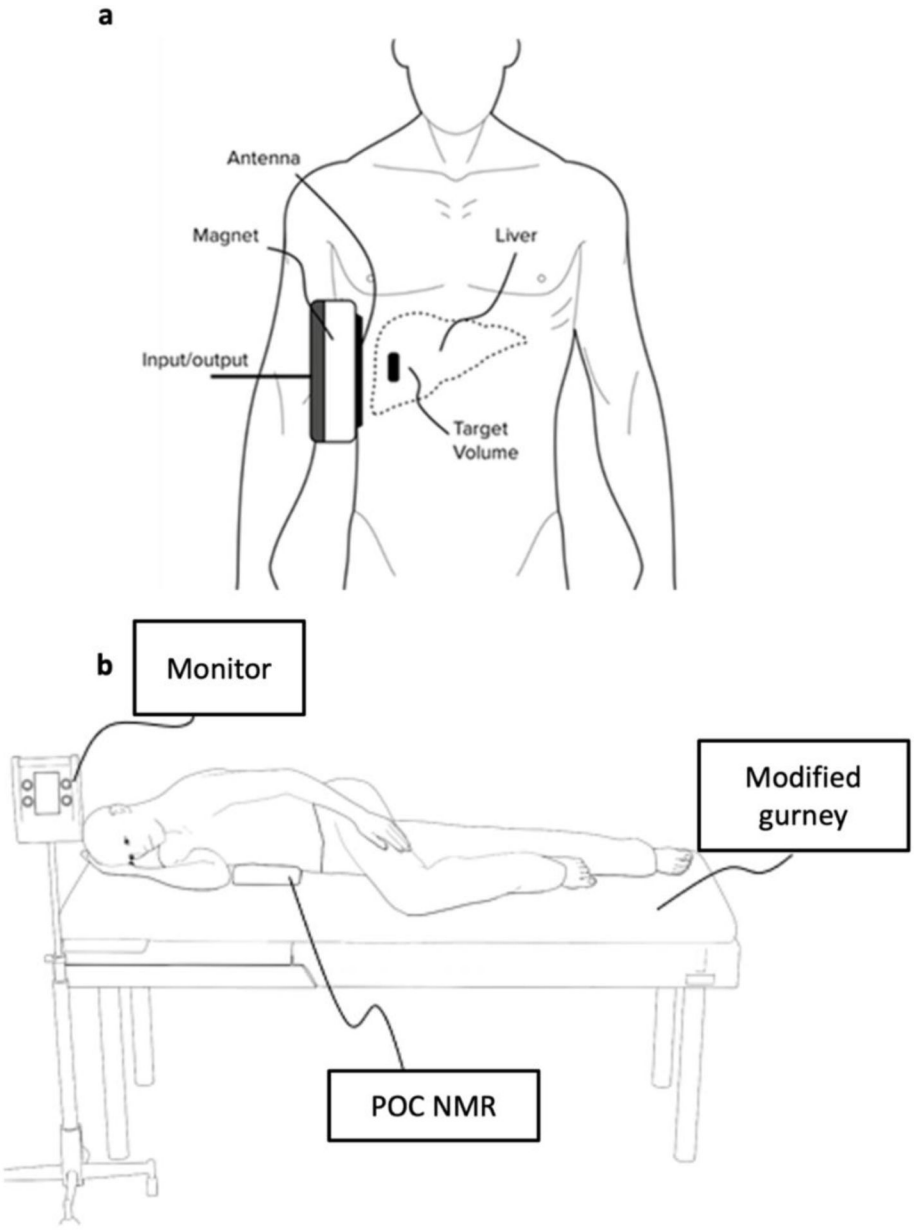

Figure 3.
POC NMR clinical examination demonstration. (a) Schematic of POC NMR device in relation to patient and liver. (b) schematic of LiverScope measurement in a human participant

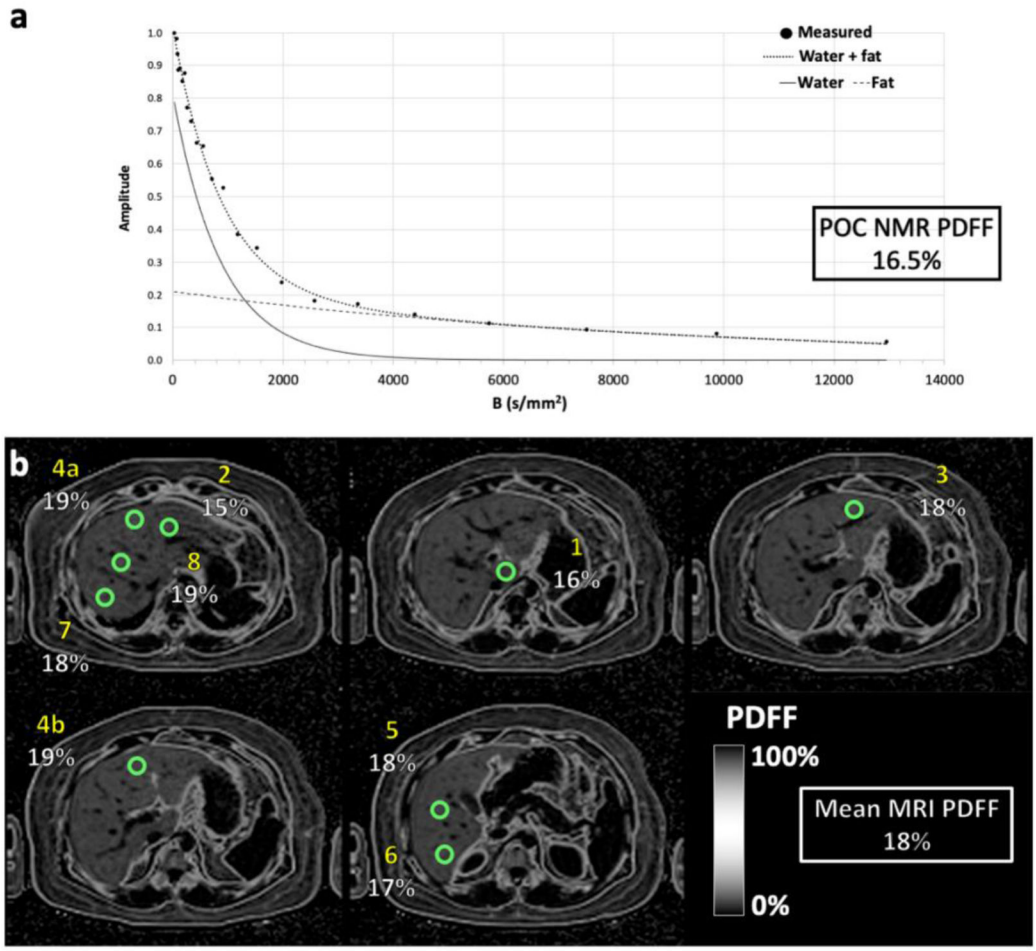

Figure 4.

(a) POC NMR PDFF determination for patient #5 using diffusion curves. Black markers represent measured signal amplitude following a diffusion encoding sequence, repeated for multiple b values. Measured data can be separated into a water diffusion curve and a fat diffusion curve. (b) MRI PDFF determination using magnitude-reconstruction based confounder-corrected chemical-shift-encoding sequence for the same patient. A mean from 9 ROIs (green circles) representing anatomical liver segments (yellow numbers) was used to calculate an average liver PDFF for each participant (white numbers).

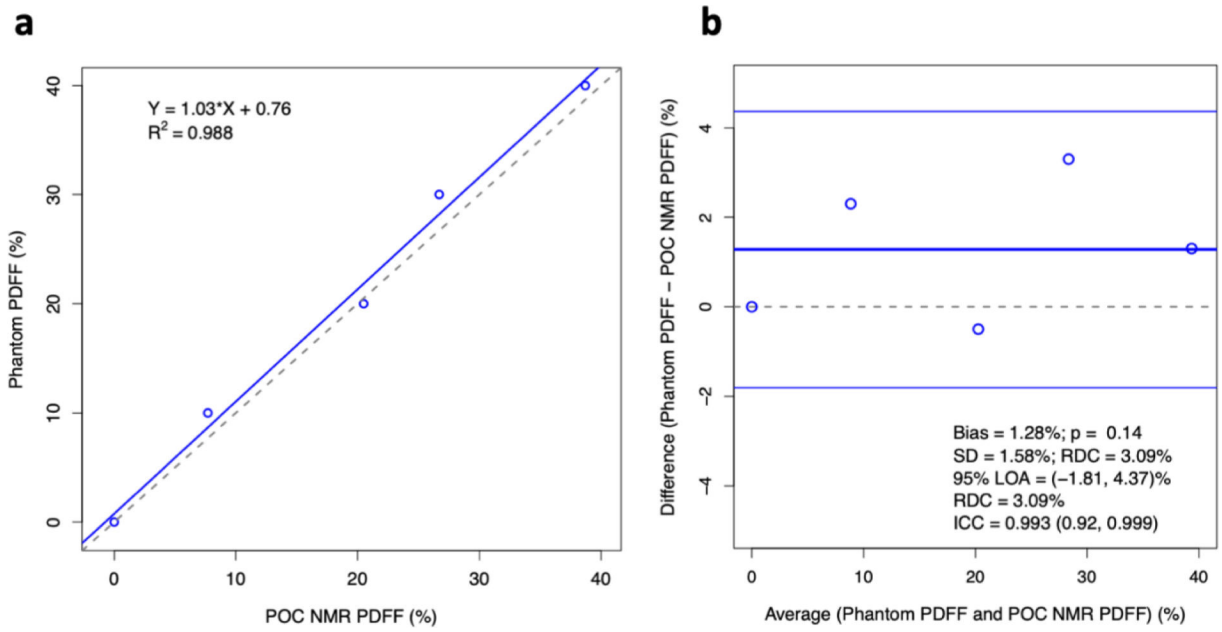

Figure 5.

POC NMR-PDFF measurements in phantoms. (a) linear regression model (blue), Identity line (grey). (b) Bland-Altman analysis.

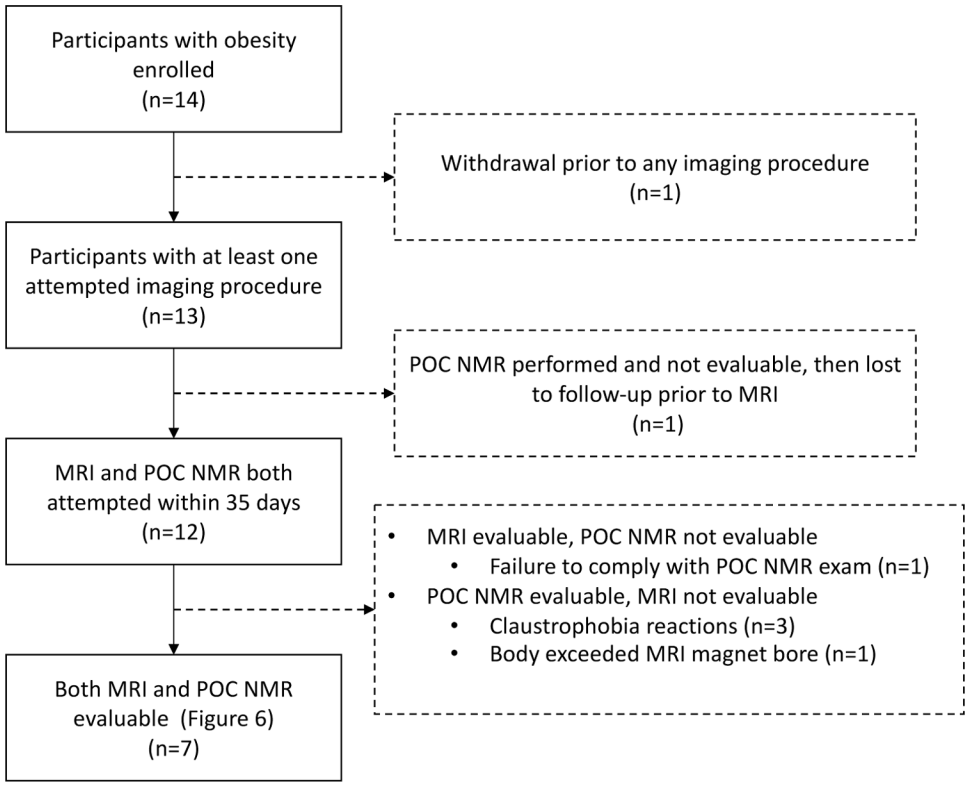

Figure 6.
Human study consort diagram

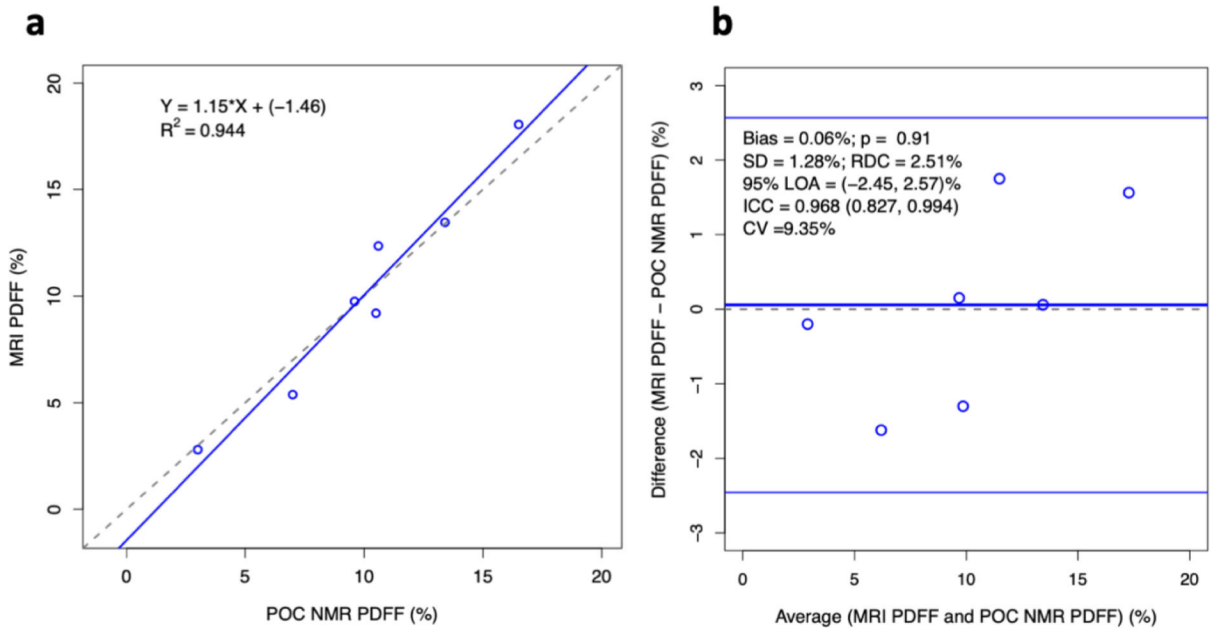

Figure 7.

MRI and POC NMR PDFF agreement in human pilot study. (a) linear regression model (blue), Identity line (grey). (b) Bland-Altman analysis. The horizontal blue line near 0 marks the bias.

Table 1.

Experimental parameters

B values [s/mm^2]	20, 55, 68, 84, 104, 131, 165, 208, 264, 336, 429, 550, 707, 911, 1177, 1525, 1981, 2577, 3360, 4387, 5739, 7519, 9863, 12955
Diffusion encoding times [ms]	1 – 8.5
Spin echo time [μs]	300
RF pulse duration [μs]	50–100
# repetitions	16

Table 2.

Participant information

ID	Gender	Age	Weight (kg)	Height (m)	BMI (kg/m^2)	Waist Circum. (cm)	SCD (cm)	MRI PDFF	POC NMR PDFF
*POC NMR evaluable, MRI evaluable									
1	F	74.0	92.3	1.6	34.4	111	4.8	9.2	9.6
2	F	69.0	79.1	1.5	34.0	103	4.4	13.5	13.4
5	F	44.0	90.6	1.6	35.4	103	3.9	9.8	9.6
7	F	62.0	76.3	1.6	31.8	104	5.8	12.4	10.6
9	M	31.0	99.4	1.7	35.9	111	5.0	18.1	16.5
10	M	40.0	136.1	1.9	36.5	129	4.1	2.8	3.0
12	M	53.0	111.6	1.8	36.3	124	5.2	5.4	7.0
mean		53.3	97.9	1.7	34.9	112.1	4.7	10.1	10.0
std		15.9	20.6	0.1	1.7	10.5	0.6	5.1	4.3
POC NMR evaluable, MRI not evaluable									
4	M	41.0	100.2	1.7	33.6	116	Fail (claustrophobia)		25.2
6	F	46.0	86.1	1.6	34.7	116	Fail (claustrophobia)		17.3
8	M	47.0	118.8	1.8	36.5	129	Fail (claustrophobia)		9.8
13	M	61.0	110.2	1.9	30.8	116	Fail (did not fit MRI)		9.0
POC NMR not evaluable, MRI evaluable									
3	F	64.0	90.7	1.5	38.1	117	6.0	17.8	Fail (exam compliance)
POC NMR not evaluable, MRI not evaluable									
11	F	38.0	104.3	1.7	36.6	112	Lost to follow up prior to MRI		Fail (did not reach liver)
mean (all participants)		49.0	93.8	1.6	32.0	106.5	4.3	9.6	11.2
std (all participants)		15.8	27.4	0.4	9.3	30.2	1.5	4.7	5.9

*Included in accuracy analysis for Figure 7.